Optimized correlations inspired by perturbation theory

Martin Panholzer,[1,2,*] Raphael Hobbiger,[1] and Helga Böhm[1]
[1]*Institute for Theoretical Physics, Johannes Kepler University Linz, Linz, Austria*
[2]*European Theoretical Spectroscopy Facility (ETSF)*

(Received 16 July 2018; revised manuscript received 3 May 2019; published 31 May 2019)

We study the accuracy of analytical wave-function-based many-body methods derived by energy minimization of a Jastrow-Feenberg ansatz for electrons (the "Fermi hypernetted chain/Euler Lagrange" approach). Approximations to avoid the complexity of the fermion problem are chosen to parallel successful boson theories and to be computationally efficient. For the three-dimensional homogeneous electron gas, we calculate the correlation energy, the pair distribution function, and the static structure function in comparison with simulation results. We also present a variant of theory which is interpreted as an approximate, self-consistent sum of ladder and ring diagrams of perturbation theory. The theory performs particularly well in the highly dilute density regime.

DOI: 10.1103/PhysRevB.99.195156

I. INTRODUCTION

The quantum many-body (MB) problem, a numerically hard problem, cannot be solved straightforwardly. A potent approximation strategy requires thoroughly understanding, for each particular system, how the relevant physics manifests itself in the existing competing theories. Here, we combine experience from three prospering fields, quantum Monte Carlo (MC), perturbation theory (PT), and variational Jastrow-Feenberg (JF) approaches [1]. We aim at a better comprehension of where, depending on the system parameters, specific approximations perform better. Our study on fermions with an only distance-dependent interaction $v(r)$ can be suitably generalized to dipoles [2], mixtures [3,4], and lattice models [5]. The homogeneous electron gas (HEG) is of particular interest because (i) it is extremely relevant for electronic structure methods, (ii) it is well studied with various methods in its entire density range, and (iii) its random-phase approximation (RPA) is well defined.

Monte Carlo methods yield benchmark results for the ground-state energy [6], the pair distribution function [7,8], and the static density-density response function [9]. Extending the applicability to excited states is an active field with utmost numerical demands [10,11].

Based on Feynman diagrams, PT is a proven systematic treatment of MB systems, widely used for calculating both excited-state [12,13] and ground-state properties [14–16]. Practical implementations allow the retaining of to retain specific, appropriately chosen classes of diagrams. A prime example is the importance of self-energy graphs for quasiparticles, successfully handled in "*GW* summations" [13,17]. Another class arises from the Bethe-Salpeter equation (BSE), relevant for correct results for exciton binding observed by optical absorption [12,18,19].

Wave-function-based methods include physical intuition right from the start, via either a parametrized or a general functional form. The Jastrow-Slater wave function, $\psi = F\phi_0$, works excellently; for homogeneous cases ϕ_0 is a plane wave Slater determinant, and $F = \prod_{i<j} \exp\left[\frac{1}{2}u_2(|r_i - r_j|)\right]$ accounts for correlations.[1] The approach attains its full power when $u_2(r)$ is optimally determined via functional variation. Inspired by cluster expansions developed for classical liquids [20], the pair distribution function $g(r)$ is here explored in the hypernetted chain formalism, abbreviated FHNC in its fermion version [21–23].

The *full* diagrammatic formalism exactly maps u_2 to all observables, as illustrated in Fig. 1 (left). Graphs are classified by their topological structure as nodal, non-nodal, or elementary diagrams. The latter are arbitrarily difficult (similar to PT, where vertex corrections are complicated). Energy minimization determines the best g via a corresponding Euler-Lagrange (EL) equation (Fig. 1, right).[2] An exact result obtained this way would essentially equal that of variational MC (VMC) with a parametrized u_2 that can reach the functional result.

The theory, like any, relies on approximations. Although not reaching quite the MC accuracy, FHNC is numerically, by orders of magnitude, less demanding.[3] It thus allows a highly efficient evaluation of observables in a multivariable space, depending, e.g., on position r, density ρ, spin σ, and valley index [24]. Most important, the FHNC can be systematically improved by topping it with PT, termed the "correlated basis function" (CBF) approach [25]. For the ground state, this is comparable to stepping from VMC to released-node diffusion MC. The CBF route is also the prime tool to extend the theory to excited states [26–31]. Again, in terms of accuracy

*martin.panholzer@jku.at

[1]The bosonic JF form is exact when correlations u_n are included to all orders.

[2]In the literature, (F)HNC may denote both the exact cluster expansion with *all* elementary diagrams and (F)HNC/0, where they are omitted. Functional optimization is emphasized by "EL," e.g., (F)HNC/0-EL.

[3]For homogeneous systems FHNC/0-EL scales as $n \ln n$ for n sampling points of $g(r)$.

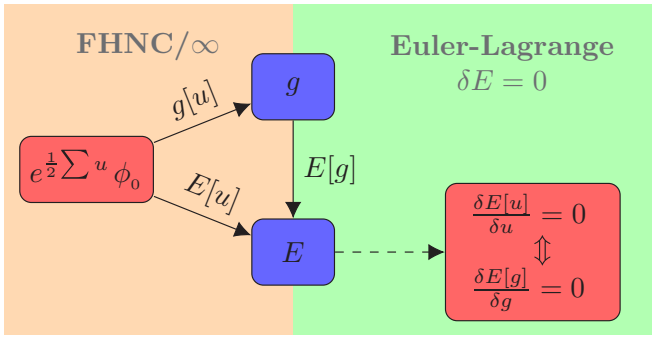

FIG. 1. Left: Graphical expansions provide an exact map from the JF correlations u_2 to the observables $g[u_2]$ (pair distribution function) and $E[u_2]$ (energy). Right: The optimal u_2 minimizes E, yielding the EL equation. This can equivalently be interpreted as a pair density functional theory.

versus computation time, obtaining dynamic properties via FHNC+CBF is much more efficient than obtaining them by MC [11,30].

At first sight, the PT and optimized JF approaches appear to be very different. Their link was demonstrated for bosons by Jackson *et al.* [32,33], who showed which approximation of the sum of parquet diagrams leads to the HNC equations. We here extend their studies to fermions. In particular, we derive an approximation to the particle-particle ladder, inherent in the variational Jastrow-Slater ansatz and identical to the boson ladder equation corrected by a "potential" constructed from the density matrix of the Slater-determinant. Accounting for self-consistently summed ladder and ring diagrams, it is excellent for highly dilute HEGs ($r_s > 5$; the density ρ is $3/4\pi\,(a_0 r_s)^3$, and a_0 is the effective Bohr radius).

We further demonstrate that this and two other FHNC variants [21,23] perform very well even in their most basic, bosonlike versions. All are easier to implement than the more often employed approach of Singwi, Tosi, Land, and Sjölander (STLS) [34] and give better results. Additionally, they yield effective interactions for PT, providing physical insight through their connection to diagrammatic (sub)classes.

II. THEORY

A. Exact EL equations

The functional variation (HNC-EL) in the case of bosons gives a Schrödinger-like equation for $\sqrt{g(r)}$, with effective potentials from sums of diagrams. Pursuing the same route for fermions makes the theory much more cumbersome: Exchange effects cause countless additional diagrams.

For bosons, if elementary diagrams are neglected (HNC/0) as their consistent treatment via two-body kernels is topologically unfeasible, two self-consistent equations arise, one being algebraic in direct space and the other one in reciprocal space. In contrast, the corresponding fermion (FHNC/0) result consists of eight plus eight coupled equations in real and reciprocal space.

This intricacy makes it difficult to identify FHNC expressions with corresponding PT diagrams. A promising route due to Krotscheck [21], ensuring the correct long-wavelength limit, is the simplified FHNC (sFHNC). Its momentum space EL equation, (A2), is understood as the sum of ring diagrams (see Appendixes A and C).

Whereas that approach is rooted in approximating the static structure factor $S(q)$ for small wave vectors q, we here derive a *real-space* formulation, arriving at a bosonlike parquet sum [33], where the ladders and rings are supplemented by a correction for Fermi statistics.

The Slater exchange function $\ell(r) \equiv l(rk_\mathrm{F})$, i.e., the density matrix of a system with Fermi momentum k_F and degeneracy factor ν, determines the noninteracting pair distribution function $g_\mathrm{F}(r) = 1 - \ell(r)/\nu$, accounting for the Pauli exclusion hole. We start with the exact FHNC expression for the pair distribution function [35],

$$g(r) = [1 + \Gamma_\mathrm{dd}(r)]\,[g_\mathrm{F}(r) + g_\mathrm{ee}(r)], \tag{1a}$$

$$g_\mathrm{ee} = 2\ell\,(N_\mathrm{cc} + E_\mathrm{cc}) - \nu(N_\mathrm{cc} + E_\mathrm{cc})^2 + N_\mathrm{ee} + E_\mathrm{ee} + 2(N_\mathrm{de} + E_\mathrm{de}) + (N_\mathrm{de} + E_\mathrm{de})^2. \tag{1b}$$

Here, we introduced the FHNC classification [36], where the capital letters N_i, X_i, and E_i denote nodal, non-nodal, and elementary diagrams and $\Gamma_i \equiv N_i + X_i$. The subscript $i \in \{\mathrm{dd}, \mathrm{de}, \mathrm{ee}, \mathrm{cc}\}$ specifies the exchange structure. Equation (1) follows from the diagrammatic rules, which also give the relations between the various ingredients. An important example arises from the dd product graphs,

$$\Gamma_\mathrm{dd}(r) = \exp\left[u_2(r) + N_\mathrm{dd}(r) + E_\mathrm{dd}(r)\right] - 1. \tag{2}$$

If all elementary graphs E_i are omitted, this route yields the first set of eight coupled FHNC/0 equations [22]. They can be solved self-consistently if u_2 in (2) is known.

To find the optimal u_2 by energy minimization, the JF ground state energy per particle e is obtained as [21]

$$e = t_0 + \frac{\rho}{2}\int d^3r\, g(r)\, V_\mathrm{JF}(r) + t_\mathrm{JF}, \tag{3a}$$

$$V_\mathrm{JF}(r) = v(r) - \frac{\hbar^2}{4m}\nabla^2 u_2(r), \tag{3b}$$

with $t_0 \equiv 3\hbar^2 k_\mathrm{F}^2/10m$ (m is a particle's mass) and where V_JF is known as the Jastrow-Feenberg interaction. The last term in Eq. (3a),

$$t_\mathrm{JF} = -\frac{\hbar^2\rho}{8m\nu}\int d^3r\, \Gamma_\mathrm{dd}(r)\, \nabla^2\ell^2(rk_\mathrm{F}) + t_\mathrm{JF}^{(3)}, \tag{3c}$$

where $t_\mathrm{JF}^{(3)} = t_\mathrm{JF}^{(3a)} + t_\mathrm{JF}^{(3b)}$ includes pair as well as three-body exchange contributions:

$$t_\mathrm{JF}^{(3a)} = \frac{\hbar^2\rho}{4m}\int d^3r\, \Gamma_\mathrm{dd}(r)\,[N_\mathrm{cc}(r) + E_\mathrm{cc}(r)]\,\nabla^2\ell(r), \tag{3d}$$

$$t_\mathrm{JF}^{(3b)} = \frac{\hbar^2\rho^2}{8m\nu^2}\int d^3r_{12} d^3r_{13}\, \Gamma_\mathrm{dcc}(\mathbf{r}_1;\mathbf{r}_2,\mathbf{r}_3)[\nabla_1\ell(r_{12})]\,[\nabla_1\ell(r_{13})] \tag{3e}$$

(∇_1 denotes differentiation with respect to $\mathbf{r}_1$); Γ_dcc collects all three-point diagrams [21], where the distinct coordinate $\mathbf{r}_1$ has no exchange line but is connected with each of $\mathbf{r}_2$ and $\mathbf{r}_3$ via a path that does not go through the respective other one, and a continuous exchange path exists between $\mathbf{r}_2$ and $\mathbf{r}_3$.

Requiring the variation of the energy with respect to u_2 to vanish leads to the EL equation

$$\frac{\hbar^2}{4m}\nabla^2 g(r) = \int d^3\bar{r}\, V_{\rm JF}(\bar{r})\frac{\delta g(\bar{\mathbf{r}})}{\delta u_2(\mathbf{r})} + \frac{2}{\rho}\frac{\delta t_{\rm JF}}{\delta u_2(\mathbf{r})} \equiv g'(r). \tag{4}$$

The right-hand side of the first line formally defines g'. It is generated diagrammatically by replacing [21], in turn, (1) every correlation line by $V_{\rm JF}(r)\,e^{u_2(r)}$ and (2) every connected pair of exchange lines by $\frac{\hbar^2}{8m}\nabla_i^2\,\ell(r_{ij})\ell(r_{ik})$. Applying these graphical rules, we obtain an expression for $g'(r)$ in terms of $\Gamma'_{\rm dd}$ and $g'_{\rm ee}$, where (as in the following) all primed quantities are constructed by employing these same rules. Inserting this definition of $\Gamma'_{\rm dd}$ and eliminating u_2 in favor of g in Eqs. (1) and (2) leads to a differential equation for g (for details, see Appendix B).

The resulting exact EL equation, (B11), is Schrödinger-like in r space,

$$\left[-\frac{\hbar^2}{m}\nabla^2 + v + w_{\rm I} + V_{\rm E} + V_{\rm ee} + V_{\rm F}\right]\sqrt{g} = 0, \tag{5}$$

where

$$V_{\rm F} \equiv \frac{\hbar^2\nabla^2\sqrt{g_{\rm F}}}{m\sqrt{g_{\rm F}}} \tag{6}$$

and $V_{\rm E}$ and $V_{\rm ee}$ denote the contribution of dd elementary diagrams and the exchange correction, respectively [see Eqs. (B7) and (B12)]. The "induced interaction" $w_{\rm I}$ [derived in (B6) and further elucidated in Appendix C] is formally defined identically to that for bosons,

$$w_{\rm I}(r) \equiv \frac{\hbar^2}{4m}\nabla^2 N_{\rm dd}(r) + N'_{\rm dd}(r). \tag{7}$$

B. Leading-order ladder FHNC-EL approach

The simplest fermionic approach is to neglect both $V_{\rm E}$ and $V_{\rm ee}$ altogether, keeping only $V_{\rm F}(r)$,

$$\left[-\frac{\hbar^2}{m}\nabla^2 + v(r) + w_{\rm I}(r) + V_{\rm F}(r)\right]\sqrt{g(r)} = 0. \tag{8}$$

All effects of the surrounding medium on a pair of particles is then contained in only two corrections to the bare $v(r)$ in (5), namely, $w_{\rm I}(r)$ induced by correlations and $V_{\rm F}$ arising from the Pauli principle.

So far, we defined $w_{\rm I}$ via the nodal diagrams. Attempting to derive an expression along this route, although further improving $g(r\to 0)$, does not change the long-wavelength behavior. We therefore choose to instead incorporate the relevant $q\to 0$ terms by using Krotscheck's sFHNC expression [21],

$$\tilde{w}_{\rm I}(q) = -\frac{\hbar^2 q^2}{4m}\left[\frac{1}{S(q)} - \frac{1}{S_{\rm F}(q)}\right]^2\left[\frac{2S(q)}{S_{\rm F}(q)} + 1\right], \tag{9}$$

with the free static structure factor $S_{\rm F}$. (As $w_{\rm I}(r)$ in (9) is finite at the origin, it ensures the cusp condition [37].)

Equations (8) and (9) constitute a closed set of equations to be solved self-consistently, correctly reproducing the noninteracting limit.

C. Relation to perturbation theory

Before presenting numerical results, we clarify the physics contained in $V_{\rm F}(r)$. Subsuming all effective interactions in $V \equiv v + w_{\rm I} + V_{\rm E} + V_{\rm ee} + V_{\rm F}$ and defining $L \equiv -\frac{\hbar^2}{m}\nabla^2(\sqrt{g}-1)$ and $t(k) \equiv \frac{\hbar^2}{2m}k^2$, the *exact* EL equation (5) reads in real and Fourier space

$$\left[-\frac{\hbar^2}{m}\nabla^2 + V(r)\right](\sqrt{g(r)}-1) + V(r) = 0,$$
$$\widetilde{L}(q) = \widetilde{V}(q) + \int\frac{d^3k}{(2\pi)^3}\,\widetilde{V}(|\mathbf{q}-\mathbf{k}|)\,\frac{\widetilde{L}(k)}{t(k)}. \tag{10}$$

This is recognized as the Bethe-Goldstone equation [38] for bosons. Recall that $V_{\rm F}$ is completely independent of interactions. Thus, even for free fermions, the FHNC-EL can be formulated as a bosonic ladder equation with a potential originating from the Slater determinant.

The similarity is no coincidence, as the optimization of the correlation function u_2 happens independently of the individual states in the Fermi sea; only their sum in the density matrix ℓ enters the optimization.[4]

Accepting the interpretation of Eq. (5) as a ladder sum, $w_{\rm I}$ is conjectured to sum the rings (bubbles) of PT. Indeed, in Appendix C we demonstrate how the sFHNC form (9) for $\tilde{w}_{\rm I}$ follows from treating the rings in the single-pole approximation. Both perspectives clearly corroborate the evidence that (8) combined with (9) is an approximate self-consistent sum of ladders as well as rings, which we therefore denote here as the "ladder$^+$ approximation."

Strategies of improvement are evident: Specifically, in every step of the self-consistency cycle one could replace the bosonic with the full fermionic propagator. This may answer which precise approximations in PT reproduce the EL equation (5). But even the present approach, derived from an alternative formalism, gives an alternative perspective and thus can open the door for new approximation schemes in PT (in particular for ladder sums), which are hard to motivate from PT alone.

D. Three bosonic FHNC-EL approaches

Note that two exact relations connect the FHNC quantities N_i and X_i with the static structure; the real-space equation (1a) and the momentum-space equation (see, e.g., Eq. (2.7) in Ref. [21]). Of course, the exact EL equation (5) for the optimal $g(r)$ from a Jastrow ansatz is equivalent to its momentum-space counterpart. Approximations, necessary in practice, usually break the equivalence of **r**- and **q**-space formulations. A crucial point here is that (the real space) Eq. (1a) with $g_{\rm ee}=0$ better approximates the ladders, whereas Eq. (A1) (in momentum space) is superior for the bubbles. We here test the performance of the following three simple, bosonlike types of FHNC/0-EL approaches: (i) ladder$^+$, a self-consistent solution of (8) and (9), (ii) sFHNC, a self-consistent solution of (A1)–(A3) and (9), and (iii) bFHNC,

[4]The $q\to 0$ expansion in sFHNC, where the fermionic Lindhard function is approximated by the bosonlike $\chi^0_{\rm CA}$, (C1), also shares this benefit of the state-independent Jastrow ansatz.

Kallio and Piilo's [23] suggestion (see below). For remarks on the implementation, see Appendix D.

On purpose and in hindsight of the theory's extension to periodic structures, we refrain from any sophisticated modifications but test the "nakedest" versions of ladder$^+$ and sFHNC. Note, however, that the Fourier transform of a good approximation for $S(q)$ from certain FHNC equations may give [39] an inadequate $g(r)$. We here stress that applications of sFHNC can be done in a refined manner (see the end of Appendix A). Our intention is to figure out where the three approaches work best, so that they can complement each other.

The version introduced by Kallio and Piilo [23] enforces the noninteracting fermion limit on the bosonic HNC-EL and was further motivated from a density functional theory (DFT) perspective [40]. For brevity, we call it bFHNC (its implementation is analogous to that of ladder$^+$; see Appendix D). This variant has been successfully applied to various charged systems before.

III. RESULTS

We now test the above approaches for the HEG. The basic assessment of a theory's accuracy is to compare the correlation energy per particle $e_c(r_s)$ with simulation results. We obtain it by coupling constant integration from the pair distribution function $g_{\bar{r}_s}(r)$ at a density parameter $\bar{r}_s$,

$$e_c(r_s) = \frac{3}{8\pi\, r_s^2} \int_0^{r_s} \frac{d\bar{r}_s}{\bar{r}_s^2} \int \frac{d^3r}{a_0^3}\, v(r)\,[g_{\bar{r}_s}(r) - g_F(r)]. \quad (11)$$

This procedure has the benefit that all three different approximations are compared on the same level, based solely on their pair distribution functions.[5]

The correlation energies of the ladder$^+$, the sFHNC, and Kallio and Piilo's bFHNC are compared to MC results in Fig. 2. The bFHNC performs best, with an error of a few percent over the whole r_s range. The sFHNC works reasonably well for metallic densities (how the deviation for $r_s \to 0$ can be corrected is reported in Appendix A). In accordance with the PT knowledge that ladder summations are crucial in the highly correlated regime [38], the ladder$^+$ curve is seen to become superior for $r_s \gtrsim 15$.

We also compare our results with the seminal BSE results of Maggio and Kresse [15]. They evaluated the four-point particle-hole ladders with a static RPA screened interaction. It appears promising to replace this by FHNC (CBF) interactions for the particle-hole ladder [28,42].

Despite the substantial simplifications of the various propagators in all three FHNC/0-EL approaches, they perform notably well. This indicates that their effective interactions are of high quality, accounting for the most relevant physics in the respective density regime.

An accurate energy does not guarantee a high-quality wave function or static structure. As is well known, the STLS [34]

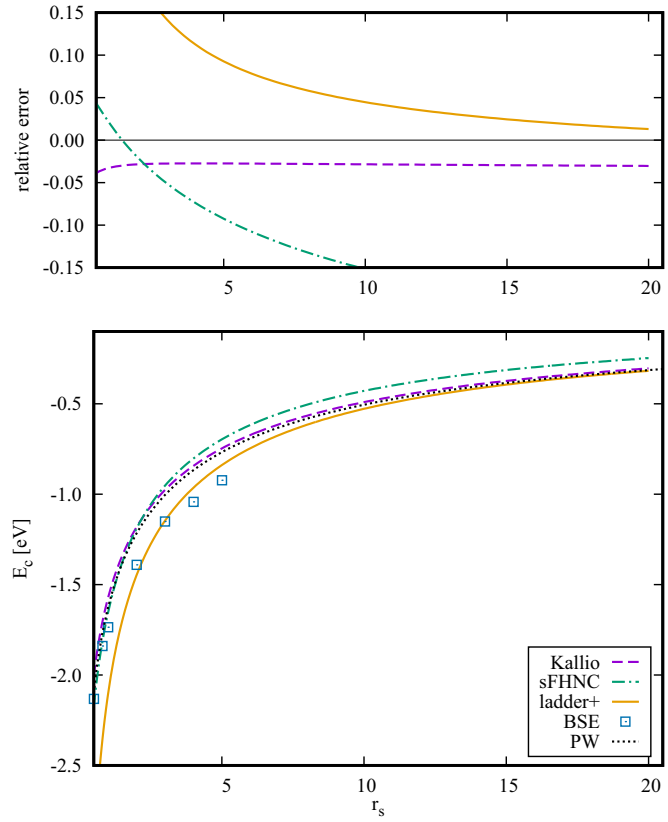

FIG. 2. Correlation energy per particle versus the density parameter for three FHNC-EL variants. Bottom: bFHNC (dashed violet line), sFHNC ring summation (dot-dashed cyan line), and the ladder$^+$ approach (solid orange line), compared to BSE [15] (squares) and parametrized MC data [6,41] (dotted black line). Top: Relative error with respect to MC.

yields excellent correlation energies but fails for $g(r \to 0)$, yielding negative values for $r_s \gtrsim 4$. The $r_s = 5$ pair distribution functions are displayed in Fig. 3; we compare them with the most recent simulations of Spink *et al.* [8]. Remarkably, the ladder$^+$ approximation is closer to MC than the bFHNC, which is high quality too. The sFHNC and STLS clearly deviate from the MC data; the inset shows that their nearest-neighbor peak position r_{m1} is dissatisfying.

Per construction, ladder$^+$ performs insufficiently for $r_s \to 0$; this error is carried over and accumulated by the coupling constant integration (11), explaining the deviations of e_c from MC. We conclude that $g(r)$ is most satisfying in ladder$^+$, but the kinetic energy is less accurate.

The fully spin polarized HEG is depicted in Fig. 4, again for $r_s = 5$. For small r the spin-polarized ladder$^+$ $g(r)$ is on top of the MC benchmark curve [8]. The behavior of the first peak position r_{m1}, foreshadowing the Wigner crystal's nearest neighbors, is interesting. The MC peak has the lowest r_{m1}; in the paramagnetic HEG the ladder$^+$ value agrees closely, and its ferromagnetic first maximum is too far right.

Note that these discrepancies are only $\sim$2%. For the two-dimensional (2D) HEG, where correlation effects are more pronounced, neglecting elementary diagrams and triplet correlations leads to larger deviations (see the review by Asgari [43]). This trend continues to one dimension, but still, the

[5]The sFHNC energy can also be directly calculated from Eq. (3); the bHNC functional is unknown. The ladder$^+$ combination of Eqs. (8) and (9) cannot be uniquely mapped on expression (3) either.

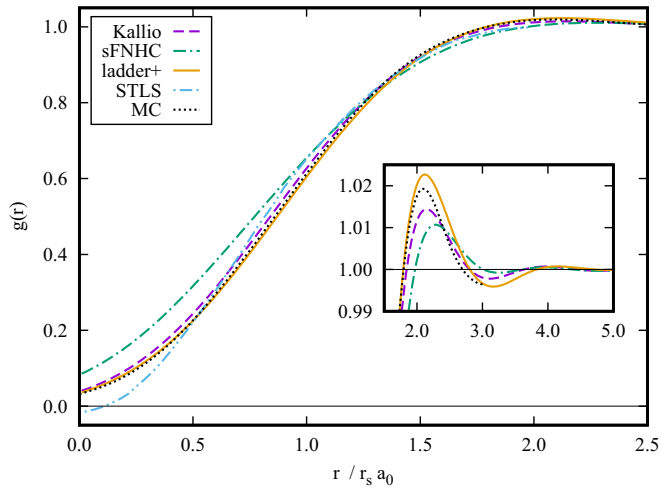

FIG. 3. Pair distribution function of the paramagnetic HEG at $r_s = 5$ in the ladder$^+$, bFHNC, and sFHNC approaches (line types as in Fig. 2), compared to a fit of MC data (Spink *et al.* [8], dotted black curve); STLS data are taken from [34] (double-dot-dashed blue line). Inset: First maximum.

ladder$^+$ serves as a reasonable starting point [44]. Similar expectations hold for partial spin polarization [45].

In Fig. 5 we compare the on-top pair distribution function $g(0)$. The overall agreement of both the ladder$^+$ and the bFHNC values with the MC results is good, with a slight superiority of the former. The static structure factor in Fig. 6 demonstrates for all approximations the correct q^2 behavior for long wavelengths, confirming the overall picture already discussed.

Of course, some of the less satisfactory features of the above approaches can be removed: Yoshizawa and Takada [47] suggested an improved STLS scheme; in sFHNC the small r behavior of $g(r)$ can be corrected as indicated at the end of Appendix A. Here, we want to compare them in their nakedest form, and it turns out that even these FHNC versions perform highly satisfactorily.

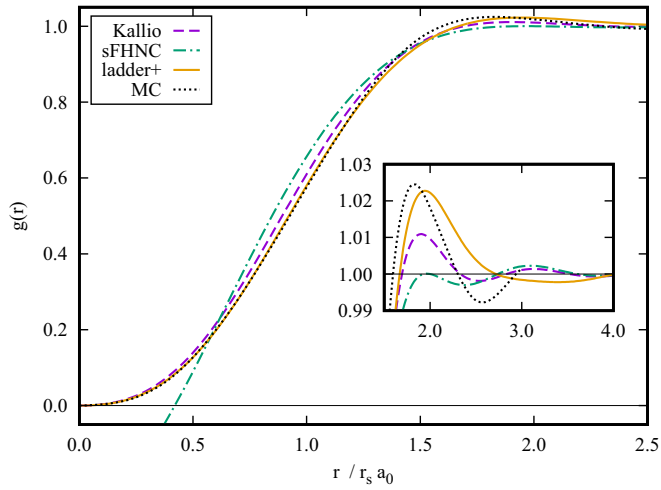

FIG. 4. Same as Fig. 3, but for the ferromagnetic HEG. The STLS curve is omitted, lying significantly below the sFHNC.

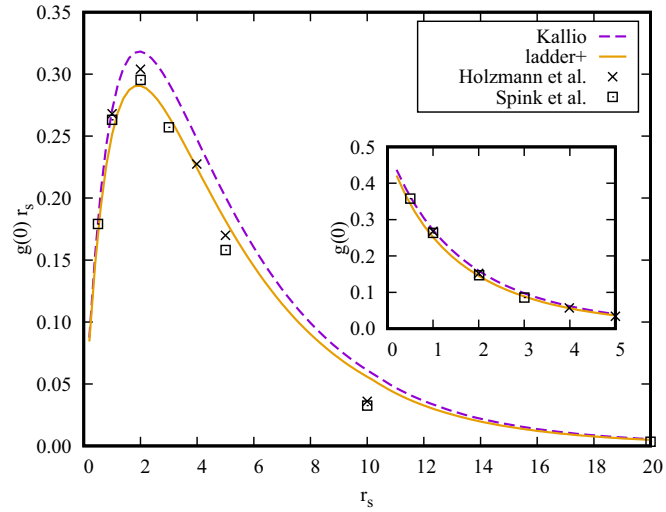

FIG. 5. On-top pair distribution function $g(0)$ multiplied by r_s for the paramagnetic HEG. The Kallio and ladder$^+$ approach is compared to the MC results of Spink *et al.* [8] and Holzmann *et al.* [46]. The inset demonstrates the correct behavior for $g(0)$ for small r_s.

Finally, in Fig. 7 we show the sum of the bare and the induced interaction, $v(r) + w_I(r)$, as this appears as the driving term in Eq. (5). Since bFHNC has an EL equation of similar form, we compare it to the corresponding expression $v + w_{IB} - w_{IBF}$ (see Appendix D). Most prominent is the minimum at $1.5 r_s a_0$, again a precursor of the Wigner crystal. Although in absolute units the minimum gets smaller with higher r_s, it has to be compared with the kinetic energy, which scales with r_s^{-2}. Thus, the effective depth becomes larger, correctly leading to a higher nearest-neighbor peak in $g(r)$.

IV. SYSTEMATIC IMPROVEMENTS

Having demonstrated that the ladder$^+$ yields generally good and, for strong correlations, excellent results, we

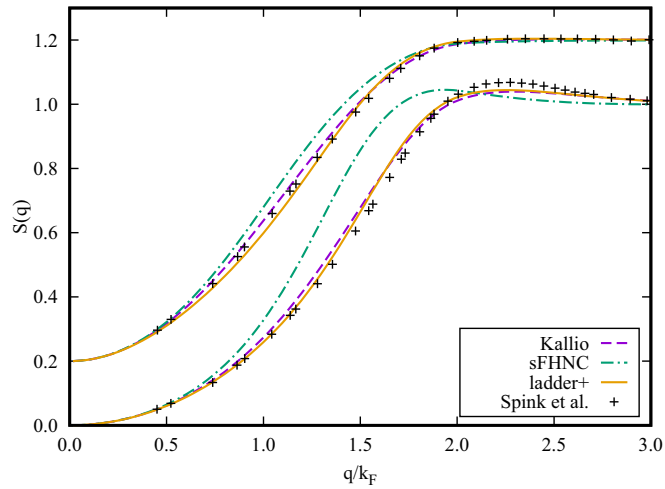

FIG. 6. The static structure function of the three FHNC approximations at $r_s = 20$ and $r_s = 5$ (shifted up by 0.2), compared to the respective MC result [8].

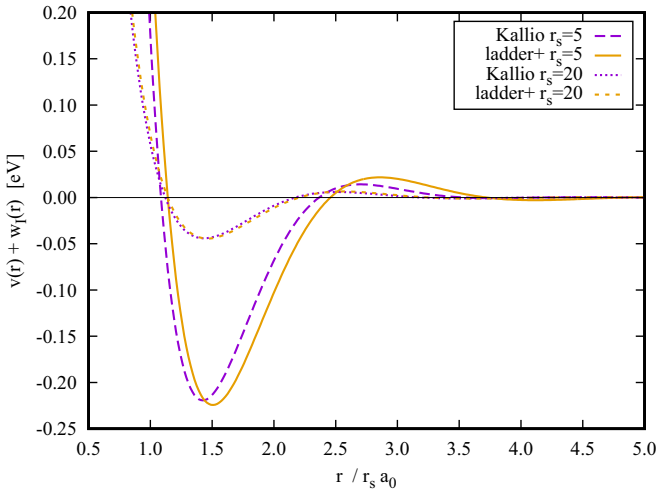

FIG. 7. Effective interaction $v(r) + w_{\rm I}(r)$ for the optimized correlations at $r_s = 5$ and $r_s = 20$. The corresponding bFHNC potential is $v + w_{\rm IB} - w_{\rm IBF}$ (see Appendix D).

here show how it can be *systematically* improved—another strength of the present theory.

A. Jastrow-Feenberg contributions

Additional diagrams. Most obvious is to include $V_{\rm ee}^0$, with the superscript 0 indicating that elementary graphs in $V_{\rm ee}$ are neglected.[6] For the nonbosonized FHNC this was done by Lantto [48], with a result similar to that of our ladder$^+$ approximation. This further justifies the simplified treatments. Including elementary diagrams is then the next step.

Higher-order correlations. Using not only pair correlations in the wave function $\psi = F\phi_0$ but adding triplet correlations $u_3(\mathbf{r}_1, \mathbf{r}_2, \mathbf{r}_3)$ (and possibly higher-order u_n) further amends the theory. The inclusion of both the diagram E_4 and triplets u_3 significantly improves the bFHNC results for the 2D HEG [43].

B. Correlated basis functions

While for bosons by adding $u_n(\mathbf{r}_1, \ldots, \mathbf{r}_n)$ of arbitrarily high order the exact ground state is reached, the unknown nodes of ψ prevent this for fermions. The CBF framework [25] remedies this problem. Particle-hole excitations of the Slater determinant, $\phi_{ph} = a_p^\dagger a_h \phi_0$, correlated by F of the FHNC ground state, form a correlated basis, allowing us to obtain the true ground state. Compared to standard PT, the CBF convergence is much faster (but derivations become more involved). We exemplify the principle of the method for the ring diagrams. Their PT summation yields the RPA. The analogous route in CBF gives the correlated RPA (cRPA) response function,

$$\chi_{\rm cRPA}(q,\omega) = \frac{\chi_0(q,\omega)}{1 - \widetilde{V}_{\rm ph}(q)\,\chi_0(q,\omega)}, \qquad (12)$$

with the bare $\tilde{v}(q)$ replaced by the particle-hole irreducible interaction $\widetilde{V}_{\rm ph} = \widetilde{X}'_{\rm dd} - \widetilde{X}_{\rm dd}\,\hbar^2 q^2/4m$. (The derivation [42] is a bit tedious; an explicit expression for $\widetilde{V}_{\rm ph}$ in sFHNC is given in Eq. (A3).)

How the induced $w_{\rm I}$ of sFHNC follows from the plasmon pole approximation of $\chi(q,\omega)$ together with the m_0 sum rule is outlined in Appendix C.[7] There, we also delineate the close relation of $\widetilde{V}_{\rm ph}$ to the ladders.

The cRPA response function (12) significantly improves the bare RPA dynamics. It should be compared to time-dependent DFT (TDDFT). An explicit nonlocal approximation for the exchange-correlation kernel is obtained via $\tilde{f}_{\rm xc} \approx \widetilde{V}_{\rm lad} = \widetilde{V}_{\rm ph} - \tilde{v}$, which should be tested against other static kernels [49,50].

Similarly, we propose an upgraded treatment of the fermionic Bethe-Goldstone equation in PT. Since $w_{\rm I}$ contains, although approximately, a large class of diagrams, using the interaction $v + w_{\rm I}$ as a driving term, the corresponding ladder sum is expected to be superior to that with the bare v and to give quicker convergence if used as a starting point in more refined summations. The latter would allow us to further assess the accuracy of the above bosonlike FHNC schemes (ideally, to be compared to a fully self-consistent sum of fermion rings and ladders, still a numerically challenging task).

Other classes of PT diagrams can be approximated by FHNC summations too. Self-energy diagrams, contained in g_{ee}, are neglected in the present treatment. Again, a combination of FHNC and PT gives good results [51].

C. Extension to inhomogeneous systems

The low computational demands of the method suggest a generalization to inhomogeneous systems. Numerically, the huge step from a one-dimensional $g(r)$ to a six-dimensional $g(\mathbf{r}, \mathbf{r}')$ makes exploiting symmetry unavoidable. As demonstrated in Ref. [44], the solution of the FHNC equations for periodic systems is numerically feasible, and further work in that direction is in progress.

Our present study adds value and reliability to that attempt. First, the relation to PT is particularly useful for describing excited-state properties of realistic systems. Second, the nonlocal behavior of two-point quantities is kept; that is, neither local nor semilocal approximations are needed, in contrast to the local density approximation (LDA) or the generalized gradient approaches in DFT. Starting from TDDFT and utilizing the adiabatic connection formula partly remove this locality with promising results [49,52]; however, the nonlocality of $f_{\rm xc}$ still has to be approximated. The inhomogeneous version of the theory yields a nonlocal $f_{\rm xc}$ at the same level of approximation as the homogeneous version. Third, it allows us to account for or estimate the different approximations done by calculating, e.g., $V_{\rm ee}^0$, low-order contributions to $V_{\rm E}$, or CBF corrections.

V. CONCLUSION

We demonstrated here the strength of uncomplicated FHNC-EL versions. Their key advantage is to be based on

[6] Consequently, $w_{\rm I}$, obtained from the FHNC equations for $N_{\rm dd}$ and $N'_{\rm dd}$, then takes a more complicated form than Eq. (9).

[7] Using the full Lindhard function does not give an explicit $\widetilde{V}_{\rm ph}(q)$.

functional optimization, thus yielding a parameter-free, unbiased result for the ground-state structure. The intricacy of the full fermion version is avoided by neglecting elementary diagrams and exchange corrections g_{ee}. The resulting self-consistency equations exhibit physical transparency and share the low computational demand with classical HNC. From a practical perspective, they are thus extremely efficient while nevertheless yielding rather accurate results.

The HEG served for testing and comparing the following specific approaches: the bFHNC formulated by Kallio and Piilo [23], the sFHNC introduced by Krotscheck [21], and an FHNC-EL version that we developed for the short-range region and the low-density limit of HEGs. It self-consistently sums approximated ladder and ring diagrams with emphasis on the former, motivating the term ladder$^+$ approach.

The bFHNC method performs best in a wide density range, yielding both a pair distribution function and correlation energy close to the MC benchmark data. For high and low densities, $g(r)$ is more accurate in sFHNC and ladder$^+$, respectively. Their additional advantage is to allow a connection with PT. Consequently, their extension to periodic systems [44] holds a high potential for an implementation in combination with PT algorithms for solid-state physics, e.g., in BSE [15].

Apart from the good performance combined with low numerical cost, we stress the following: Although derivations in the FHNC-EL formalism are intricate, they *justify* the resulting equations and energy functionals. Once established, these can then be applied in a pair DFT [40,53–55], the pair analog of conventional DFT.

Finally, the possibility of coherently refining the method via CBF and generalizing the static ground-state correlations to dynamic fluctuations [27,29] underpins the value and utility of the FHNC approach.

ACKNOWLEDGMENT

The research was supported by the Austrian science fund FWF under Project No. J 3855-N27.

APPENDIX A: sFHNC

We provide a brief summary of the sFHNC as formulated by Krotscheck [21]. The static structure factor S and its noninteracting counterpart S_F are related to the sum of all direct-direct cluster diagrams $\widetilde{\Gamma}_{dd}$ via

$$S(q) = S_F(q)\,[1 + S_F(q)\,\widetilde{\Gamma}_{dd}(q)], \tag{A1}$$

which is exact for $q \to 0$. Denoting the energy of a free single particle as $t(q) \equiv \hbar^2 q^2/2m$, the EL equation resulting from minimizing the ground-state energy reads

$$S(q) = \frac{S_F(q)}{\sqrt{1 + \frac{2S_F^2(q)}{t(q)}\widetilde{V}_{ph}^{sFHNC}(q)}}, \tag{A2}$$

with the particle-hole irreducible interaction [21]

$$V_{ph}^{sFHNC}(r) = [1 + \Gamma_{dd}(r)]\,v(r) + \frac{\hbar^2}{m}\left|\nabla\sqrt{1+\Gamma_{dd}(r)}\right|^2 + \Gamma_{dd}(r)\,w_I(r). \tag{A3}$$

Here, w_I is related to the summed nodal diagrams exactly as in (7). Consistent with the approximations leading to (A1), $\tilde{w}_I$ can be expressed in terms of the static structure function, resulting in Eq. (9). From $\Gamma_{dd}(r)$ the potential V_{ph}^{sFHNC} is obtained with (A3), yielding $S(q)$ via (A2) and then $\widetilde{\Gamma}_{dd}$ for the next iteration step from (A1).

We emphasize that also the sFHNC contains both ring and ladder diagrams in V_{ph}^{sFHNC}, Eq. (A3), and that these are summed in an approximate but *consistent* way.

As Krotscheck [39] pointed out, the Fourier transform (FT) of $S(q)$ does not yield a physically meaningful $g(r)$. Instead, g should be calculated differently, or additional FHNC integral equations should be included for the exchange diagrams. The importance of the latter, alternatively, can be estimated by comparing a good $g(r)$ with the FT of $S(q)$.

Since Eq. (A1) is designed to exactly reproduce the FHNC $q \to 0$ limit, the small r regime may well lack quality. Specifically, $g(r \to 0)$ is not well approximated and violates the cusp condition.

An *ad hoc* recipe [56] is to obtain g from Eq. (1a) with $g_{ee} = 0$, i.e., $g = (1 + \Gamma_{dd})\,g_F$, as it holds in ladder$^+$, but with $\Gamma_{dd}(r)$ being the FT of $\widetilde{\Gamma}_{dd} = (S - S_F)S_F^{-2}$. We do not use this for the following reasons: First, it violates the most fundamental relation between $S(q)$ and $g(r)$, Eq. (D6). Second, although improving $g(r \to 0)$, the result gets much worse for intermediate distances, $r \gtrsim 0.5\,r_s a_0$, in the present case of Coulomb systems. Third, this additional assumption spoils the simplicity and elegance of the original approach.

APPENDIX B: DETAILED DERIVATION OF THE EULER LAGRANGE EQUATION

We provide here all contributions to the exact FHNC-EL theory. Like in Ref. [57], we stay in real space, but in contrast to their usage of Lagrange multipliers in the optimization procedure, we employ the diagrammatic rules.

To get familiar with the formalism, we demonstrate the explicit procedure for obtaining the primed Γ'_{dd} by applying the graphic rules defined in Sec. II to the unprimed Γ_{dd} in Eq. (2). First, we replace $e^{u_2} - 1$ by $V_{JF}\,e^{u_2}$. Then we need to utilize both rules for the collection of N_{dd} and E_{dd} graphs, thus defining N'_{dd} and E'_{dd} as sums of specific diagrams. Rewriting

$$\Gamma_{dd} = (e^{u_2} - 1)\big(1 + N_{dd} + \tfrac{1}{2}N_{dd}^2 + \cdots\big)e^{E_{dd}} + \big(1 + N_{dd} + \tfrac{1}{2}N_{dd}^2 + \cdots\big)e^{E_{dd}} - 1, \tag{B1}$$

it is straightforward to apply rule 1 directly, and both rules to all subdiagrams.[8] Explicit expressions are obtained by invoking the rules in the FHNC equation for N_{dd} and the chosen approximation to E_{dd}.

To keep the derivation general, we continue with the exact expression. Collecting all product graphs leads to

$$\Gamma'_{dd} = (1 + \Gamma_{dd})\,(V_{JF} + N'_{dd} + E'_{dd}). \tag{B2}$$

This is applied analogously to all FHNC equations. With the underlying definition being based on a functional derivative,

[8]The rules are used in turn for each subdiagram; for example, applied to $N_{dd}^2/2$, they give $N_{dd}N_{dd'}$.

this mostly amounts to taking the "ordinary" derivative of each equation, where all new primed ingredients are well-defined diagrammatic sums. When g'_{ee} is obtained graphically, the execution of rule 2 for two connected cc diagrams requires some care (in the literature often avoided by neglecting $t_{JF}^{(3b)}$, argued to be negligibly small). Some pertinent details are discussed at the end of this section.

For g' obtained from (1a),

$$g' = \Gamma'_{dd}\,(g_F + g_{ee}) + (1+\Gamma_{dd})\left(\frac{\hbar^2}{4m}\nabla^2 g_F + g'_{ee}\right), \tag{B3}$$

we can now rewrite the first term with (B2) as

$$\Gamma'_{dd}\,(g_F + g_{ee}) = g\,(V_{JF} + N'_{dd} + E'_{dd}). \tag{B4}$$

Here, we replace u_2 in V_{JF} with Eq. (1) by

$$u_2 = \ln\left(\frac{g}{g_F + g_{ee}}\right) - N_{dd} - E_{dd}, \tag{B5}$$

and obtain for the right-hand side of Eq. (B4),

$$\begin{aligned} &g\left\{v - \frac{\hbar^2}{4m}\nabla^2\left[\ln\left(\frac{g}{g_F+g_{ee}}\right) - N_{dd} - E_{dd}\right] + N'_{dd} + E'_{dd}\right\} \\ &\quad\equiv g\left[v - \frac{\hbar^2}{4m}\nabla^2 \ln\left(\frac{g}{g_F+g_{ee}}\right) + w_I + V_E\right]. \end{aligned} \tag{B6}$$

This proves Eq. (7) for the induced potential w_I and gives an analogous expression for another effective interaction,

$$V_E = \frac{\hbar^2}{4m}\nabla^2 E_{dd} + E'_{dd}, \tag{B7}$$

due to dd elementary diagrams. Although coinciding with the bosonic formulas, w_I and V_E contain many more diagrams arising from the various internal exchange lines.

Using the identity

$$\nabla^2 g + g\,\nabla^2 \ln g = 4\sqrt{g}\,\nabla^2\sqrt{g}, \tag{B8}$$

the exact EL equation (4) takes the form

$$\begin{aligned} 0 &= \left(\frac{\hbar^2}{4m}\nabla^2 g - g'\right)\Big/\sqrt{g} \\ &= \frac{\hbar^2}{m}\nabla^2\sqrt{g} - \sqrt{g}\left[v + w_I + V_E + \frac{\hbar^2}{4m}\nabla^2 \ln\,(g_F+g_{ee})\right. \\ &\quad\left.\times\,\frac{1}{g_F+g_{ee}}\left(\frac{\hbar^2}{4m}\nabla^2 g_F + g'_{ee}\right)\right], \end{aligned} \tag{B9}$$

where Γ_{dd} on the right-hand side of (B3) has been expressed with g_{ee}.

We intentionally separate the exchange contributions into the *purely statistical* g_F and the *correlation-dominated* V_{ee},

$$\begin{aligned} \ln\,(g_F+g_{ee}) &= \ln g_F + \ln\,(1+g_{ee}/g_F), \\ \frac{1}{g_F+g_{ee}} &= \frac{1}{g_F} + \left(\frac{1}{g_F+g_{ee}} - \frac{1}{g_F}\right). \end{aligned} \tag{B10}$$

Collecting all terms and applying (B8) to g_F lead to

$$\frac{\hbar^2}{m}\nabla^2\sqrt{g} = \left(v + w_I + V_E + V_{ee} + \frac{\hbar^2}{m}\frac{\nabla^2\sqrt{g_F}}{\sqrt{g_F}}\right)\sqrt{g}, \tag{B11}$$

with the exchange correction

$$\begin{aligned} V_{ee} = \frac{\hbar^2}{4m}\nabla^2 \ln\left(1 + \frac{g_{ee}}{g_F}\right) + \frac{g'_{ee}/g_F}{1+g_{ee}/g_F} \\ - \frac{g_{ee}/g_F}{1+g_{ee}/g_F}\left(\frac{\hbar^2}{4m}\frac{\nabla^2 g_F}{g_F}\right). \end{aligned} \tag{B12}$$

The $\sqrt{g_F}$ term in (B11) can be viewed as a simple Fermi correction to the bosonic ladder (propagator) equation, in analogy to sFHNC, which is an approximation to PT ring diagrams with the Lindhard function replaced by the simpler collective approximation [see (C1)].

As mentioned above, employing rule 2 may appear cumbersome. This is avoided by neglecting $t_{JF}^{(3b)}$, which leads to a simplified (approximate) form of rule 2: In turn, each loop formed by two exchange lines is replaced with $\frac{\hbar^2}{4m}\nabla^2\ell(r)^2$, and where more than two such lines make a loop, each exchange line, in turn, is replaced by $\frac{\hbar^2}{4m}\nabla^2\ell(r)$. Within this approximation we obtain

$$\begin{aligned} g'_{ee} \approx 2[\ell + v(N_{cc}+E_{cc})](N'_{cc}+E'_{cc}) + (N_{cc}+E_{cc})\frac{\hbar^2}{m}\nabla^2\ell \\ + N'_{ee} + E'_{ee} + 2[1 + N_{de} + E_{de}](N'_{de}+E'_{de}). \end{aligned} \tag{B13}$$

Together with some specific approximation for the elementary diagrams, this provides an explicit expression for V_{ee} in (B12) if the ladder$^+$ approach is taken a step further.

APPENDIX C: DERIVATION OF w_I FROM PT

Here, we demonstrate how the induced potential w_I is obtained from the ring (=bubble) diagrams of PT. As a first step the Lindhard function is approximated in the "collective" (or "single-pole") approximation,

$$\chi_0^{CA}(q,\omega) = \frac{2t(q)}{(\hbar\omega + i\eta)^2 - [t(q)/S_F(q)]^2}, \tag{C1}$$

implying an RPA response of Bijl-Feynman form,

$$\chi_{RPA}^{CA}(q,\omega) = \frac{\chi_0^{CA}(q,\omega)}{1 - \tilde{v}(q)\,\chi_0^{CA}(q,\omega)}. \tag{C2}$$

This approximation will elucidate the physical meaning of w_I. We next add, in a similar spirit, a two-point approximation of the ladder diagrams to the bare interaction, $v \to v + V_{lad} \equiv V_{ph}$. Note that the rungs in V_{lad} are not just bare, but rather a consistently resummed interaction, justifying the identification with the particle-hole irreducible diagrams (no specific V_{lad} needs to be assumed here). The m_0 sum rule (or adiabatic connection) relates V_{ph} to the static structure:

$$S(q) = -\int_0^\infty d\hbar\omega \mathrm{Im}\left[\chi_{cRPA}^{CA}(q,\omega)\right] = \frac{t(q)}{\epsilon(q)}, \tag{C3a}$$

$$\epsilon(q)^2 \equiv \frac{t(q)^2}{S_F(q)^2} + 2t(q)\,\widetilde{V}_{ph}(q). \tag{C3b}$$

This is identical to the sFHNC EL equation (A2).

The ring diagrams generated from $\widetilde{V}_{ph}(q)$ are

$$\widetilde{V}_{ring}(q,\omega) \equiv \frac{\widetilde{V}_{ph}(q)^2\,\chi_0^{CA}(q,\omega)}{1 - \widetilde{V}_{ph}(q)\,\chi_0^{CA}(q,\omega)}. \tag{C4}$$

Even though $\widetilde{V}_{\rm ph}(q)$ is static, this summation is energy dependent. Following Jackson *et al.* [33] we replace ω in $V_{\rm ring}$ by a suitably determined characteristic frequency $\bar{\omega}_q$. Again, the solely statistical effects are split off,

$$\chi(q,\omega) = \chi_0(q,\omega) \; + \; \chi_0^2(q,\omega)[\,\widetilde{V}_{\rm ph}(q) + \widetilde{V}_{\rm ring}(q,\omega)] \approx \chi_0^{\rm CA}(q,\omega) + \chi_0^{\rm CA}(q,\omega)^2[\widetilde{V}_{\rm ph}(q) + \widetilde{V}_{\rm ring}(q,\bar{\omega}_q)]\,. \tag{C5}$$

Demanding consistency with the static structure implies

$$S(q) \; = \; S_{\rm F}(q) - \frac{S_{\rm F}(q)^3}{t(q)} \, \frac{\widetilde{V}_{\rm ph}(q)}{1 - \widetilde{V}_{\rm ph}(q)\, \chi_0^{\rm CA}(q,\bar{\omega}_q)}. \tag{C6a}$$

This results in (we skip q for ease of reading)

$$\widetilde{V}_{\rm ph}\, \chi_0^{\rm CA}(\bar{\omega}_q) \; = \; 1 - \frac{S_{\rm F}}{2S}\left[\frac{S_{\rm F}}{S} + 1\right]; \tag{C6b}$$

solving for $\bar{\omega}_q$ using (C3) gives

$$\hbar^2 \bar{\omega}_q^2 \; = \; -\frac{\epsilon(q)\, t(q)^2 / S_{\rm F}^2(q)}{\epsilon(q) + 2t(q)/S_{\rm F}^2(q)}, \tag{C6c}$$

the fermion analog of the boson $\bar{\omega}_q$ found in Ref. [33].

Inserting (C6b) into (C4), we thus have shown that

$$\widetilde{w}_{\rm I}(q) = \widetilde{V}_{\rm ring}(q,\bar{\omega}_q); \tag{C7}$$

that is, $w_{\rm I}$ in Eq. (9) is indeed the sum of approximated ring diagrams with the effective interaction $v + V_{\rm lad}$.

This procedure also explains the name "induced potential" for $w_{\rm I}$. Defined as the difference between the screened and bare interactions, $\tilde{v}_{\rm ind}$ in plain RPA is

$$\tilde{v}_{\rm ind} \; = \; \frac{\tilde{v}}{1 - \tilde{v}\, \chi_0} - \tilde{v} \; = \; \frac{\tilde{v}\, \chi_0\, \tilde{v}}{1 - \tilde{v}\, \chi_0}. \tag{C8}$$

Replacing the bare interaction by the particle-hole irreducible interaction demonstrates the connection.

APPENDIX D: IMPLEMENTATION

We show here a favorable self-consistent procedure to treat bosonlike FHNC equations. Instead of numerically solving the nonlinear differential equation (5), a straightforward manipulation maps it onto an algebraic relation in reciprocal space. The static structure factor defines an auxiliary potential, where we split off the boson-induced interaction,

$$S(q) \equiv 1/\sqrt{1 + \frac{2}{t(q)}\widetilde{V}_{\rm aux}(q)}, \tag{D1a}$$

$$\widetilde{w}_{\rm IB}(q) \equiv -\frac{t(q)}{2}\left[\frac{1}{S(q)} - 1\right]^2 [2S(q) + 1], \tag{D1b}$$

$$\widetilde{V}_{\rm aux}(q) = -\widetilde{w}_{\rm IB}(q) - \, t(q)(S(q) - 1). \tag{D1c}$$

In the exact EL equation multiplied by $\sqrt{g}$, where (as in Sec. II C) we subsume all effective interactions in V,

$$\left[-\frac{\hbar^2}{m}\nabla^2 + V(r)\right] g(r) + \frac{\hbar^2}{m}\left|\nabla\sqrt{g(r)}\right|^2 \; = \; 0, \tag{D2}$$

the term Vg is recognized as $-V_{\rm aux} - w_{\rm IB}$, so that the auxiliary potential in real space is

$$V_{\rm aux}(r) = V(r)\, g(r) \; - \; w_{\rm IB}(r) + \frac{\hbar^2}{m}\left|\nabla\sqrt{g(r)}\right|^2. \tag{D3}$$

In the ladder$^+$ approximation the explicit expression reads

$$V_{\rm aux}^{\rm lad^+}(r) = \left[v(r) + w_{\rm I}(r) + \frac{\hbar^2\nabla^2\sqrt{g_{\rm F}(r)}}{m\sqrt{g_{\rm F}(r)}}\right] g(r) - w_{\rm IB}(r) + \frac{\hbar^2}{m}|\nabla\sqrt{g(r)}|^2. \tag{D4}$$

An initial guess for $g(r)$ gives $V_{\rm aux}(r)$ from (D4) and, in turn, after a Fourier transform (FT) with the convention

$$\widetilde{V}_{\rm aux}(q) \; = \; \rho \int d^3r\, e^{-i\mathbf{q}\cdot\mathbf{r}}\, V_{\rm aux}(r) \tag{D5}$$

a static structure factor from (D1a), inserted into (D1b). The inverse FT gives $w_{\rm IB}(r)$ and a new $g(r)$ from

$$g(r) - 1 \; = \; \int \frac{d^3q}{(2\pi)^3\rho}\, e^{i\mathbf{q}\cdot\mathbf{r}}\, [S(q) - 1]. \tag{D6}$$

This procedure is iterated until convergence is achieved, merely having the FT as a rate-limiting step. Note that in contrast to STLS-type [34] methods, all FHNC-EL approaches presented here are easier to implement since no integrations other than the FT are involved.

For the bFHNC of Kallio and Piilo we adopt the same strategy. The auxiliary potential acquires an additional term, $w_{\rm IBF}$, which is determined solely by $S_{\rm F}$,

$$V_{\rm aux}^{\rm Kallio}(r) = [v(r) + w_{\rm IB}(r) - w_{\rm IBF}(r) + \, V_{\rm F}(r)]\, g(r) - w_{\rm IB}(r) + \frac{\hbar^2}{m}|\nabla\sqrt{g(r)}|^2,$$

$$\widetilde{w}_{\rm IBF}(q) \; \equiv -\frac{1}{2}t(q)\left[\frac{1}{S_{\rm F}(q)} - 1\right]^2 [2S_{\rm F}(q) + 1]. \tag{D7}$$

This corresponds to approximating the exact real-space EL equation (5) with

$$\left[-\frac{\hbar^2}{m}\nabla^2 + v + w_{\rm IB} - w_{\rm IBF} + V_{\rm F}\right]\sqrt{g(r)} = 0. \tag{D8}$$

For $v \to 0$, the iterations yield $w_{\rm IB} \to w_{\rm IBF}$. An appealing feature is that this concept can be easily extended to include elementary diagrams.

An implementation of all three versions discussed in the present work, the sFHNC, the bFHNC, and the ladder$^+$ method can be found in Ref. [58].

[1] A. Fabrocini, S. Fantoni, and E. Krotscheck, *Introduction to Modern Methods of Quantum Many-Body Theory and Their Applications*, Series on Advances in Quantum Many-Body Theory Vol. 7 (World Scientific, River Edge, NJ, 2002), p. 413.

[2] A. Macia, D. Hufnagl, F. Mazzanti, J. Boronat, and R. E. Zillich, Phys. Rev. Lett. **109**, 235307 (2012).

[3] C. Staudinger, F. Mazzanti, and R. E. Zillich, Phys. Rev. A **98**, 023633 (2018).

[4] E. Krotscheck, M. Saarela, K. Schörkhuber, and R. Zillich, Phys. Rev. Lett. **80**, 4709 (1998).

[5] X. Q. G. Wang, S. Fantoni, E. Tosatti, and L. Yu, Phys. Rev. B **41**, 11479 (1990).

[6] D. M. Ceperley and B. J. Alder, Phys. Rev. Lett. **45**, 566 (1980).

[7] P. Gori-Giorgi, F. Sacchetti, and G. B. Bachelet, Phys. Rev. B **61**, 7353 (2000).

[8] G. G. Spink, R. J. Needs, and N. D. Drummond, Phys. Rev. B **88**, 085121 (2013).

[9] S. Moroni, D. M. Ceperley, and G. Senatore, Phys. Rev. Lett. **75**, 689 (1995).

[10] M. Motta, D. E. Galli, S. Moroni, and E. Vitali, J. Chem. Phys. **143**, 164108 (2015).

[11] M. Nava, D. E. Galli, S. Moroni, and E. Vitali, Phys. Rev. B **87**, 144506 (2013).

[12] M. Rohlfing and S. G. Louie, Phys. Rev. B **62**, 4927 (2000).

[13] G. Onida, L. Reining, and A. Rubio, Rev. Mod. Phys. **74**, 601 (2002).

[14] B. Holm and F. Aryasetiawan, Phys. Rev. B **62**, 4858 (2000).

[15] E. Maggio and G. Kresse, Phys. Rev. B **93**, 235113 (2016).

[16] F. Bechstedt, Phys. Rev. B **97**, 241109(R) (2018).

[17] F. Aryasetiawan and O. Gunnarsson, Rep. Prog. Phys. **61**, 237 (1998).

[18] S. Albrecht, L. Reining, R. Del Sole, and G. Onida, Phys. Rev. Lett. **80**, 4510 (1998).

[19] M. Gatti and F. Sottile, Phys. Rev. B **88**, 155113 (2013).

[20] J.-P. Hansen and I. R. McDonald, *Theory of Simple Liquids: With Applications to Soft Matter* (Academic Press, Oxford, 2013), p. 619.

[21] E. Krotscheck, J. Low Temp. Phys. **119**, 103 (2000).

[22] A. Polls and F. Mazzanti, in *Introduction to Modern Methods of Quantum Many-Body Theory and Their Applications* (Ref. [1]), pp. 49–119.

[23] A. Kallio and J. Piilo, Phys. Rev. Lett. **77**, 4237 (1996).

[24] O. Gunawan, Y. P. Shkolnikov, K. Vakili, T. Gokmen, E. P. De Poortere, and M. Shayegan, Phys. Rev. Lett. **97**, 186404 (2006).

[25] E. Krotscheck, in *Introduction to Modern Methods of Quantum Many-Body Theory and Their Applications* (Ref. [1]), pp. 267–330.

[26] H. Godfrin, M. Meschke, H.-J. Lauter, A. Sultan, H. M. Böhm, E. Krotscheck, and M. Panholzer, Nature (London) **483**, 576 (2012).

[27] H. M. Böhm, R. Holler, E. Krotscheck, and M. Panholzer, Phys. Rev. B **82**, 224505 (2010).

[28] M. Panholzer, H. M. Böhm, R. Holler, and E. Krotscheck, J. Low Temp. Phys. **158**, 135 (2010).

[29] M. Panholzer, M. Gatti, and L. Reining, Phys. Rev. Lett. **120**, 166402 (2018).

[30] G. E. Astrakharchik, R. E. Zillich, F. Mazzanti, and J. Boronat, Phys. Rev. A **94**, 063630 (2016).

[31] E. Akaturk, S. H. Abedinpour, and B. Tanatar, J. Phys. Commun. **2**, 015018 (2018).

[32] A. D. Jackson, A. Lande, and R. A. Smith, Phys. Rep. **86**, 55 (1982).

[33] A. D. Jackson, A. Lande, and R. A. Smith, Phys. Rev. Lett. **54**, 1469 (1985).

[34] K. S. Singwi, M. P. Tosi, R. H. Land, and A. Sjölander, Phys. Rev. **176**, 589 (1968).

[35] S. Fantoni and S. Rosati, Nuovo Cimento A **25**, 593 (1975).

[36] J. W. Clark, Prog. Part. Nucl. Phys. **2**, 89 (1979).

[37] J. C. Kimball, Phys. Rev. A **7**, 1648 (1973).

[38] E. Lipparini, *Modern Many-Particle Physics* (World Scientific, Singapore, 2003), p. 72.

[39] E. Krotscheck, Nucl. Phys. **A293**, 293 (1977).

[40] B. Davoudi, R. Asgari, M. Polini, and M. P. Tosi, Phys. Rev. B **68**, 155112 (2003).

[41] J. P. Perdew and Y. Wang, Phys. Rev. B **45**, 13244 (1992).

[42] M. Panholzer, Ph.D. thesis, Johannes Kepler University, 2010.

[43] R. Asgari, Iran. J. Phys. Res. **8**, 87 (2008).

[44] M. Panholzer, J. Low Temp. Phys. **187**, 639 (2017).

[45] D. Kreil, C. Staudinger, K. Astleithner, and H. M. Böhm, Contrib. Plasma Phys. **58**, 179 (2018).

[46] M. Holzmann, B. Bernu, C. Pierleoni, J. McMinis, D. M. Ceperley, V. Olevano, and L. D. Site, Phys. Rev. Lett. **107**, 110402 (2011).

[47] K. Yoshizawa and Y. Takada, J. Phys.: Condens. Matter **21**, 064204 (2009).

[48] L. J. Lantto, Phys. Rev. B **22**, 1380 (1980).

[49] T. Olsen and K. S. Thygesen, Phys. Rev. B **88**, 115131 (2013).

[50] M. Corradini, R. Del Sole, G. Onida, and M. Palummo, Phys. Rev. B **57**, 14569 (1998).

[51] I. Seydi, S. H. Abedinpour, R. Asgari, and B. Tanatar, Phys. Rev. A **98**, 063623 (2018).

[52] C. E. Patrick and K. S. Thygesen, J. Chem. Phys. **143**, 102802 (2015).

[53] E. Krotscheck, Phys. Lett. A **190**, 201 (1994).

[54] F. Furche, Phys. Rev. A **70**, 022514 (2004).

[55] M. Higuchi and K. Higuchi, Comput. Theor. Chem. **1003**, 91 (2013).

[56] J. Egger, E. Krotscheck, and R. E. Zillich, J. Low Temp. Phys. **165**, 275 (2011).

[57] L. J. Lantto and P. J. Siemens, Phys. Lett. B **68**, 308 (1977).

[58] The implementation is available at https://github.com/mpanho/FHNC_3D.git.